Maximizing energy transfer in vibrofluidized granular systems

C. R. K. Windows-Yule,[1] A. D. Rosato,[2] D. J. Parker,[1] and A. R. Thornton[3]

[1]*School of Physics and Astronomy, University of Birmingham, Edgbaston, Birmingham B15 2TT, United Kingdom*

[2]*Department of Mechanical Engineering, New Jersey Institute of Technology, Newark, New Jersey 07102, USA*

[3]*Multiscale Mechanics (MSM) and Mathematics of Computational Science (MaCS), (MESA+), CTW, University of Twente, P.O. Box 217, 7500 AE Enschede, The Netherlands*

(Received 14 October 2014; published 22 May 2015)

Using discrete particle simulations validated by experimental data acquired using the positron emission particle tracking technique, we study the efficiency of energy transfer from a vibrating wall to a system of discrete, macroscopic particles. We demonstrate that even for a *fixed input energy* from the wall, energy conveyed to the granular system under excitation may vary significantly dependent on the frequency and amplitude of the driving oscillations. We investigate the manner in which the efficiency with which energy is transferred to the system depends on the system variables and determine the key control parameters governing the optimization of this energy transfer. A mechanism capable of explaining our results is proposed, and the implications of our findings in the research field of granular dynamics as well as their possible utilization in industrial applications are discussed.

DOI: 10.1103/PhysRevE.91.052203 PACS number(s): 81.05.Rm, 34.50.Ez, 45.70.Mg

I. INTRODUCTION

Granular systems—conglomerations of individual, macroscopic particles—play various important roles in multitudinous natural [1–3] and industrial [4,5] phenomena. Granular materials are distinct from classical, molecular materials due largely to the inherently dissipative nature of their dynamical interactions. In contrast to molecular systems, if a granular system is to maintain a kinetic state, a constant influx of energy is required—without a continuous energy source, a granular fluid will quickly collapse into an immobile, solid-like state [6].

Energy may be provided to a granular system in a variety of different manners; here, we focus on energy injection through contact with a vibrating wall, a mechanism directly relevant to numerous industrial applications, ranging from the processing of pharmaceuticals, to the conveying, drying, agglomeration, and milling of materials in the food industry and even the safe and efficient disposal of hazardous waste [7–11].

The state and dynamical behavior of a given vibrofluidized granular system may be quantified by two dimensionless quantities: the energy input (or "shaking strength") parameter, $S = \frac{4\pi^2 f^2 A^2}{gd}$, and the dimensionless acceleration, $\Gamma = \frac{4\pi^2 f^2 A}{g}$. Using discrete particle method (DPM) simulations supported by experimental data, we explore how altering the frequency, f, and amplitude, A, of the oscillations energizing a granulate may impact the efficiency with which energy is transferred into the system. It is demonstrated that even if the input energy, S, with which the system is driven remains constant, by varying the specific combination of f and A (and hence Γ) used to produce a given S, one may produce a substantial increase in the internal energy of the granulate being vibrated. We show this observation to be robust, persisting over a considerable range of energy inputs, S, and bed depths, N_L,[1] illustrating how the frequency-amplitude combination producing maximal energy transfer varies dependent on these parameters.

Our findings carry several noteworthy consequences; most notably, an ability to control the efficiency with which energy is transferred to a granulate may be beneficial in terms of energy-saving and cost-reduction in industrial processes where the fluidization of granular materials is a prerequisite. A knowledge of the combination of parameters which may, for a given system, be expected to produce a maximal absorption of energy by a granulate is also potentially of value in the design of granular dampers, an emerging technology with applications ranging from the improvement of surgical and dental tools [12] to the construction of skyscrapers [13].

The results of this study also highlight the necessity for researchers to consider the interrelation of the control parameters governing a system's behavior—when conducting a study aiming to investigate the dependence of a system's behavior on, say, the driving *energy*, one must also account for effects arising due to the inevitable variation of f, A, and/or Γ; worryingly, one does not need to look hard to discover a research paper where such considerations are inevident.

In this paper, we begin by presenting details of the system under investigation (Sec. II A), before providing an explanation of how experimental data is acquired (Sec. II B) and how the system is recreated using discrete particle method (DPM) simulations (Sec. II C). In Sec. III, we present and interpret our data and finally, in Sec. IV, we summarize our findings.

II. MATERIALS AND METHODS

A. Experimental setup

Our general experimental apparatus consists of an 80-mm square-based container of height 200 mm in which a granular bed of $256 < N < 2560$ spherical steel particles, each of

[1]For the purposes of this paper, we use the symbol N_L to represent the number of layers, or bed depth, as opposed to the symbol F, with which some readers may be more familiar. This choice of nomenclature is intended to maximise clarity due to the frequent usage of the lowercase f to represent driving frequency.

diameter $d = 5 \pm 0.005$ mm, is housed. The container is affixed to an electrodynamic shaker, allowing the system to be vibrated sinusoidally in the vertical (z) direction. The frequency, f, and amplitude, A, of these sinusoidal oscillations are varied in the ranges $7.96 \leqslant f \leqslant 119.4$ Hz and $0.4 \leqslant A \leqslant 6.0$ mm, respectively, allowing us to access a broad spectrum of driving accelerations and energies. In order to assess the variation in the efficiency with which energy is transferred from the container's vibrating base plate to the granular medium housed within, the peak vibrational velocity, $v = \frac{\omega A}{\sqrt{gd}}$, and hence the input energy, S, is held constant, with a series of data sets being taken using differing combinations of A and f to produce this same, fixed value of the driving energy S. For each of these groups of experiments, all other system variables are held constant. This process is then repeated for various energy inputs and particle numbers.

The height of the system is adequately large that particle collisions with the system's upper boundary are highly improbable for the range of N and S used, meaning that the system can be considered effectively open. The relatively large particle diameter allows the effects of interstitial air to be neglected [14], and this considerable size combined with the use of a stainless steel base plate minimizes the influence of triboelectric charge within the system [15].

In the following sections, the "size" of our system is quantified by the dimensionless bed height, N_L (defined as the vertical extent of the static bed normalized by the diameter, d, of a single particle), as opposed to the total particle number, N. The choice to present our data in terms of N_L arises due to the fact that this parameter is, for a given particle elasticity, generally accepted as the relevant energy-dissipation control parameter for systems such as those explored here [16–18]; indeed, the suitability of N_L (and, similarly, the inappropriateness of N) as a control parameter is directly demonstrated in Sec. III.

The vertical sidewalls that bound the system in the horizontal directions are deliberately chosen to be smooth, and a relatively low aspect ratio, $\mathcal{A} = \frac{N_L}{L_{x,y}/d}$, is maintained for all data sets ($\forall N : \mathcal{A} < 1$), thus reducing the probability of convective motion within the bed [19]. The absence of convection within our system was confirmed through analysis of two-dimensional velocity fields [20], which, through the observed random distribution of particle velocities, clearly demonstrated a distinct lack of coordinated or bulk motion within the bed [21]. Although, as will become clear in subsequent sections, the presence of convection would not be expected to significantly influence the phenomena that form the focus of this study, the elimination of convective motion nonetheless allows us to more easily study the behaviours of our systems on a more fundamental level.

The sinusoidal oscillations used to excite the system are controlled via a feedback loop from an accelerometer; as such, the system's dimensionless acceleration is accurate to within $\Gamma = 0.005$.

B. Data acquisition—positron emission particle tracking

Data is acquired from the system described above using positron emission particle tracking (PEPT), a noninvasive technique capable of tracking a single particle, in three-dimensions, with millimeter-scale accuracy and a temporal resolution of the order of milliseconds [22]. PEPT is performed by radioactively labeling a single "tracer" particle, physically identical to all others in the bed, with a β^+-emitting radioisotope, causing it to produce γ-ray pairs whose orientations are separated by 180°. Through the detection of several such pairs of γ rays using a dual-headed γ camera, the tracer's spatial position can be triangulated. Thus, for an adequately active tracer, a rapid succession of these triangulation events allows its motion to be tracked. Since the 511 keV γ rays emitted by the tracer are highly penetrating, particle motion can be recorded even in the interior of deep, dense, and/or opaque systems.

Although PEPT only directly measures the motion of a single particle, for systems in a nonequilibrium steady state, and if data is obtained over an adequately long period, the principle of ergodicity means that the time-averaged behavior of this single tracer may be considered representative of that of the system as a whole [23]. Thus, PEPT may be used to accurately determine various important quantities pertaining to the granular system and its dynamics, such as packing density [23], kinetic energy (and the fluctuations and spatial variations thereof) [24], particle velocities and velocity distributions [25], mean-squared displacement and diffusion coefficients [26] and, for systems comprising more than one "species" of particle, the degree of segregation exhibited [27].

Due to the reliance of the PEPT technique on the existence of an ergodic steady state, care is taken to ensure that, in all cases, the behavior of the granular systems explored remains consistent throughout the duration of each recorded data set. For each run, the bed is excited for an initial period of 1000 s in order to allow a steady state to be reached; this particular time period is chosen as it has been previously shown to be more than adequate to successfully produce a steady state in systems similar to those explored here [20]. Data is then recorded over a period of between 3600 s and 7200 s, dependent on the size of the system, and hence the time required for the tracer to fully explore the experimental volume. The steady state nature of the system is subsequently confirmed by subdividing each run into a series of overlapping 200- to 400-s segments and ensuring consistency between each segment. Although it is difficult to directly "test" the ergodicity of our experimental system, if the particle density distributions produced from each 200- to 400-s time segment are compared to those corresponding to the full data set as well a results acquired for the equivalent simulated system (see Sec. II C below) and agreement is observed in all cases, it is likely that the system described is indeed ergodic. In fact, based on this criterion, our systems can be assumed ergodic even for the highest-density systems explored in this paper, although, as touched upon previously, the densest systems require a considerably longer run time than the most dilute in order to fully explore the system. Further validation of the ergodicity assumption for more densely packed systems was conducted using discrete particle simulations; details regarding the manner in which these further tests were performed may be found in the next section.

C. Simulations

In order to elucidate and verify the various trends and behaviors observed in our experimental data, simulations were

performed using the MercuryDPM software package [28–31]. In order to emulate as accurately as possible the experimental setup, parameters including f and A (and hence Γ and S), the particle number, N, diameter, d, and material density, $\rho = 7850\,\mathrm{kgm}^{-3}$, as well as the container dimensions ($L_{x,y,z}$) were implemented as their known experimental values. Particle-particle, particle-base, and particle-sidewall collisions were all modeled with experimentally obtained coefficients of restitution $\varepsilon_p = 0.80$, $\varepsilon_b = 0.75$, and $\varepsilon_w = 0.59$, respectively. The coefficient of friction, μ, was taken as 0.12 [32]. Although not included here for the sake of brevity, full details of the MercuryDPM code may be found in the references provided above or, alternatively, in the Supplemental Material of our previous paper [27].

Since, as discussed above, more densely packed systems are more likely to exhibit a lack of ergodicity, additional tests of the ergodicity assumption were conducted using simulations, where ensemble averages of whole beds and long-time averages of single-particle behaviors can be directly compared. Specifically, a series of simulations spanning the range of S and N_L used in experiment was produced. For each simulation, two sets of steady-state temperature and density fields were produced—one attained by time-averaging the motion of a single particle and the other through a simple time- and ensemble-average across all particles. Although the run duration required for the time-averaged single particle behavior to be truly representative of the whole system varied considerably over the range of parameters tested, the ergodicity assumption was found to hold for all systems explored, lending a considerable degree of support to the validity of our experimental data acquired using PEPT.

III. RESULTS AND DISCUSSION

In order to quantify the average internal energy possessed by a given granular system, we calculate the time-averaged position of its vertical center of mass, h, which—due to the relation $E_P = Mgh$ (with M the total mass of the particulate assembly and g the acceleration due to gravity)—provides a measure of the system's potential energy. Specifically, we choose a parameter $h^* = \frac{h-h_0}{h_0}$, the relative increase in the system's center of mass from its resting ($S = 0$) state. Here, h_0 represents the center of mass of the relevant static bed. Confirmation of the viability of h^* as a measure of the system's internal energy may be seen in Fig. 1, which shows data for a simulated system of dimensionless depth $N_L = 4$ driven with a fixed input energy $S = 3.26$. This image clearly demonstrates the close correspondence between the variation with f and A of h^* and that of the system's total internal energy, E_T, i.e., the time-averaged sum of the average kinetic[2] (E_K) and gravitational potential (E_P) energies for all particles in the system. This close correspondence in the forms of the observed trends is found to persist across the full range of parameters tested, with Fig. 1 simply providing a convenient visual illustration of this fact. Although values of h^* and E_T

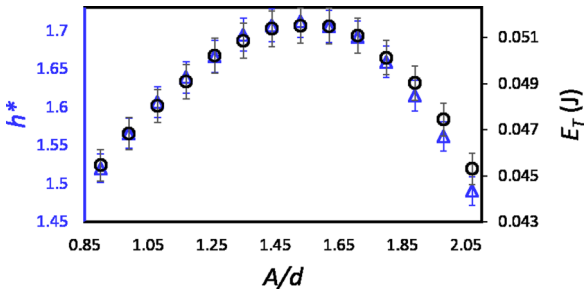

FIG. 1. (Color online) Comparison of the variation with the nondimensionalized driving amplitude, A/d, of h^*, the relative increase in a system's center of mass height from its resting position (blue triangles), and E_T, the total energy (kinetic and potential) possessed by the system (black circles), as determined from simulations.

clearly do not possess a direct, 1:1 equivalence, importantly, they *can* be expected to present maxima and minima at the same points in phase space, and indeed the same relative increasing or decreasing trends between these extrema, and it is these (as opposed to any absolute numerical values) that form the focus of our present work.

Although at first glance the strong correlation between the observed trends in the time-averaged, steady-state values of h^* and E_T may seem surprising, it is not necessarily unexpected. Since, in vibrated systems such as ours, $E_T = E_K + E_P$ and $E_P \propto h^*$, the observed correlation simply implies that the remaining component, E_K, must be proportional to E_P and hence h^*, an idea supported by existing theory [33], as well as our own results.[3]

Perhaps the most striking feature of the data shown in Fig. 1, however, is the considerable variation in the system's internal energy, despite the fact that both N_L and S are fixed—in direct contradiction of our expectations based on previous experimental and theoretical studies [34,35]. The possible origins of this discrepancy will be discussed in detail later in this section.

The decision to represent, throughout this manuscript, the variation in system energy using h^* arises from the fact that while h^* may be determined with a high degree of accuracy from both PEPT data and simulations, the accuracy with which our experimental techniques can determine E_K is less than desirable for relatively dense systems. Thus, in order to guarantee both accuracy and ease of comparison across the full range of systems explored, data is predominantly presented in terms of h^*.

The average center of mass position can be extracted from PEPT data as follows: the computational volume corresponding to the experimental system is divided into a series of equally sized cells in the vertical direction. The fractional residence time of the tracer particle within each of these cells can then be determined. Due to the principle of ergodicity, this averaged residence time is directly proportional to the

[2] E_K includes kinetic energy in both the translational and rotational modes, ensuring that E_T is an accurate representation of the system's total energy.

[3] It is important to note that the various energy and center of mass values quoted throughout this manuscript refer—unless otherwise specified—to *time-averages* taken from systems in their steady states.

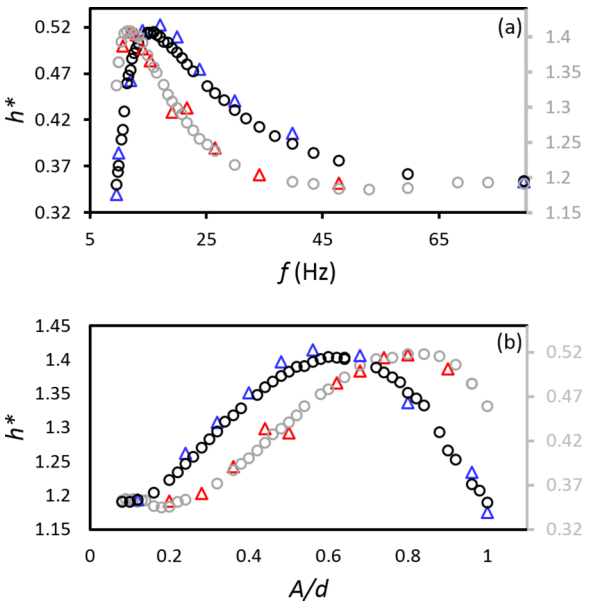

FIG. 2. (Color online) Variation of the relative increase in center of mass, h^*, with frequency and amplitude at a fixed dimensionless input energy $S = 1.83$. Data is shown for both experimental (triangles) and simulated (circles) data sets and for two differing bed heights: $N_L = 3$ (gray circles and red triangles) and $N_L = 6$ (black circles and blue triangles). Panel (a) shows the variation in h^* as a function of driving *frequency*, f, while panel (b) plots h^* against the dimensionless driving *amplitude*, $\frac{A}{d}$, where d is the diameter of a particle.

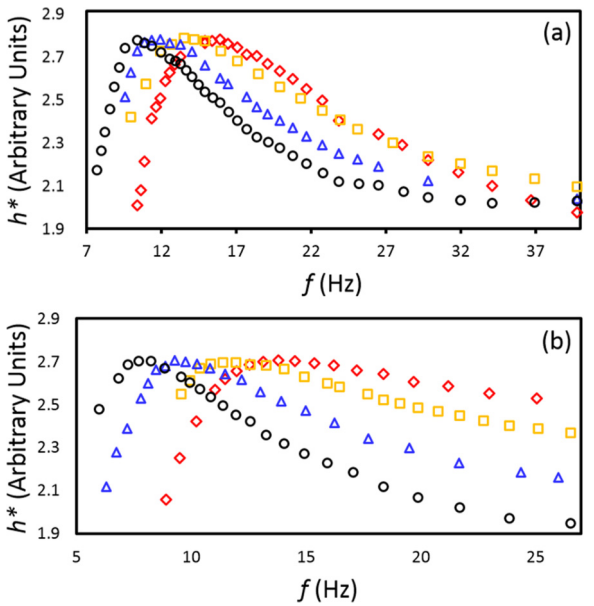

FIG. 3. (Color online) Center of mass position for simulated beds as a function of frequency, f, for a variety of differing bed heights, N_L, and driving energies, S, produced via simulation. The center of mass positions for each N_L-S combination have been arbitrarily normalized such that the positions of the various maxima may be easily compared by visual inspection. Panel (a) shows data for a fixed driving strength $S = 1.83$ for beds of depth $N_L = 2$ (circles), $N_L = 3$ (triangles), $N_L = 4$ (squares), and $N_L = 6$ (diamonds). Panel (b) gives data for a constant bed height $N_L = 3$ driven with input energy $S = 1.37$ (diamonds), $S = 1.83$ (squares), $S = 2.75$ (triangles), and $S = 4.13$ (circles).

average particle density within each of these vertical cells. With a known particle density at each given height within the container, the system's time-averaged vertical center of mass can then be easily determined.

Figure 2 shows, for both experiment and simulation, how, for a *single, fixed input energy* $S = 1.83$, the systems's center of mass heights (and hence *internal energies*) are observed to change as f and A are varied by a decade. Data is shown for two systems, identical in all aspects other than the number of particles forming the bed, and hence their approximate resting bed heights, $N_L = \frac{Nd^2}{L_x L_y}$.

The most obvious, and rather remarkable, observation to be drawn from Fig. 2 is the *significant variation* in the system's internal energy, which, considering the unaltered driving energy, implies a considerable change in the efficiency with which energy is transferred into the system. Indeed, for the $N_L = 6$ case shown, simply through adjustment of the combination of f and A used to produce the fixed value of S, h^* can be increased by almost 50% above the "baseline" value that it asymptotically approaches in the large f, small A limit. In other words, since h^* is directly representative of the energy supplied to the bed by the base vibrations, we are observing a ~50% increase in the efficiency of this energy transfer in the optimal case. Equally large—and even greater—increases in the efficiency of energy transfer can also be seen for numerous other values of the dimensionless bed depth, N_L, and shaking strength, S.

A second notable feature of Fig. 1 is the similarity between the general trends in the variation of h^* for both cases. Indeed, this same typical form is adhered to over a range of bed depths, N_L, and driving strengths, S, as made apparent by the simulated results shown in Fig. 3. Specifically, our experiments and simulations strongly imply that the behavior discussed in this manuscript may be expected to hold as long as the system under investigation is adequately dilute and strongly excited to allow fluid-like dynamics. The observed behavior seemingly breaks down only when the bed undergoes a phase transition to the less kinetic "bouncing bed" [36] state and begins to move as a single, solid body. At this point, the introduction of resonances between base motion and the solid-like bed's free flight time introduce additional variation in energy transfer to the system [37], resulting in more complex dynamics.

Having established that the trend between h^* and the system's driving parameters is robust across a range of bed heights and driving strengths, we now attempt to explain the mechanisms underlying this behavior. We begin by discussing the initial increase in h^* with increasing amplitude (decreasing frequency) for small A (large f). Figure 4 shows how the average rate of collision, ν_b, between grains and the system's energy-providing base plate varies as a function of the plate's peak amplitude, A, for a fixed input energy $S = 1.83$ and a bed of dimensionless depth $N_L = 2$. The image clearly demonstrates a significant, monotonic increase in the frequency of base-particle interactions as amplitude is increased at fixed S. Since the plate's mean velocity is fixed and, as illustrated in the diagram, the average duration of the contact between a single particle and the plate is approximately invariant with A, one would naturally expect an increase in

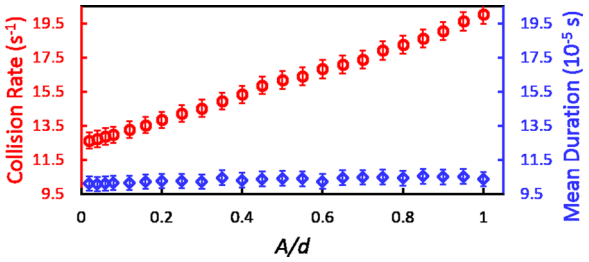

FIG. 4. (Color online) Mean collision rate (circles) and contact time (diamonds) for particle-base interactions as a function of driving amplitude, A, for a fixed base vibrational energy $S = 1.83$. Data shown is acquired from DPM simulations and corresponds to the case $N_L = 2$. Each data point represents an average taken over ~100 000 individual collisions.

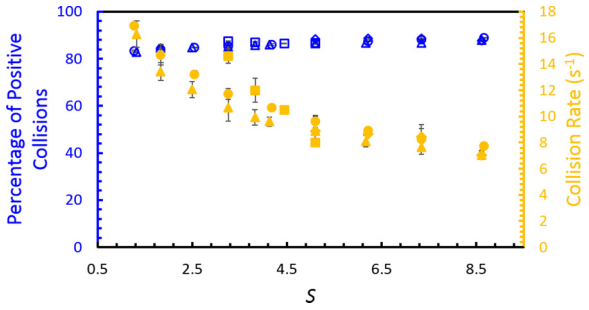

FIG. 5. (Color online) Particle-base collision rate per particle [solid orange (light gray) symbols] and the percentage of these collisions that occur when the base's motion is in the positive vertical (upward) direction [open blue (dark gray) symbols] as a function of the vibrational energy parameter S. Data is shown for the case of constant acceleration with $\Gamma = 8$ (circles) and $\Gamma = 13.5$ (triangles) as well as for parameter combinations producing a constant $h^* = 2.1$ (squares) and $h^* = 2.8$ (diamonds). In all cases, the resting bed depth is fixed at a value $N_L = 3$. The extent in S of the fixed-h^* data sets is constrained by the limited overlap between the ranges of center of mass positions achievable for differing S-values—for example, the lowest h^* achievable in a system driven with $S = 7.34$ is still greater than the largest obtainable h^* value for an equivalent system with $S = 3.26$.

the rate of collisions to lead to an increase in the energy transferred to the granular medium as a whole [38]. It is interesting to note that the considerable variation in collision rate observed for a fixed value of base velocity, v, achieved using different combinations of f and A is in stark contrast to the observations of Falcon *et al.* [35] and Aumaitre and Fauve [34], who show, both experimentally and theoretically, a direct proportionality between v_b and $v = \sqrt{S}$ implying that, for fixed S and N, v_b should remain constant. The strongly differing behaviors observed in our simulations can perhaps be explained by the relatively inhomogeneous distribution of particles in our system compared to those belonging to the dilute, low-gravity environments explored in Refs. [34,35]. The relatively small vibrational amplitudes used in these prior studies may also play a contributing role in the observed differences, as other studies [39] utilizing larger vibrational amplitudes have observed near-linear increases in collision rate similar to those described here.

Another important factor to bear in mind when considering the efficiency of energy transfer between a vibrating surface and a system of particles is that as well as *providing* energy to colliding particles, particle-base interactions may also act to *remove* particles' kinetic energy if collisions occur while the base undergoes the downward phase of its oscillatory cycle. As the velocity, v_p, of a particle within the system increases relative to the base's velocity, such energy-reducing collisions become increasingly prevalent [40,41]. Indeed, in the limit $v \to \infty$, one may anticipate that, for finite base velocity, the net energy input to the system will actually tend to zero! Since the scaling relation between a system's average particle velocity, $\langle v_p \rangle$, and base velocity, $v = \sqrt{S}$, is not precisely known [33,42–44], it is important to investigate not only the typical frequency of particle-base collisions, as described above, but also the relative proportion of these collisions that occur when the base is ascending and descending as this, clearly, will influence the net energy input to the system.

Figure 5 shows the variation with S of the likelihood that a given particle will experience an energy-augmenting collision with the upward-moving base (a "positive collision") as opposed to an energy-removing interaction with the base during its downward phase (a "negative collision"). The measured fraction of positive collisions shows, for fixed Γ, a slow increase with S. This is an interesting observation, as it gives us some insight into the scaling of the average particle velocity, $\langle v_p \rangle$—and hence the system's mean kinetic energy or "granular temperature"—with the peak base velocity v [38]. Specifically, while a relation $\langle v_p \rangle \propto v^\alpha$ with $\alpha = 1$ is often assumed in theoretical models [33,42], the increasing trend of Fig. 5 suggests an increasing disparity between $\langle v_p \rangle$ and v as S increases, i.e., $\alpha < 1$. Although this matter is not a main focus of the current study, it is nonetheless worth mentioning, due to the considerable importance of such scaling relations to the theoretical modeling of granular flows [45].

For the purposes of the present work, the presence of the trend discussed above can be quite safely neglected as, over the range of variables investigated, the variation in the positive collision probability is dwarfed by that of the total collision rate—while the percentage of positive collisions is found to change by less than 10% between the extremal cases investigated, the collision rate varies by more than a factor of three. Thus, this latter parameter may indeed be expected to dominate the energy transfer behaviors of our systems as discussed above.

If the above conjecture regarding the increasing particle-base collision rate with increasing driving amplitude, A, is indeed valid, one might expect the positive correlation between h^* and driving amplitude to continue *ad infinitum*. However, as Figs. 1– 3 clearly demonstrate, this is not the case. A clue as to the origin of this somewhat unexpected downturn at large A (small f) may be provided by replotting the data from Fig. 3(b) as a function of the dimensionless acceleration, Γ (see Fig. 6). In this image we see that, unlike when plotted as a function of f, the positions of the maxima of h^* for each S value are approximately coincident. It should be noted, however, that the same does not apply for differing N_L values, as will be discussed below. Another interesting observation to be drawn from this Figure is that stronger driving, in general, elicits a greater disparity between the maximal value

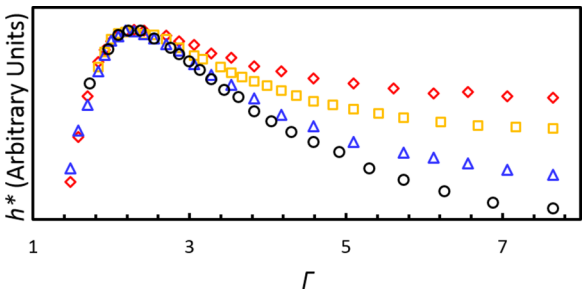

FIG. 6. (Color online) Simulated data showing center of mass position as a function of dimensionless acceleration, Γ, for various fixed input energies: $S = 1.37$ (diamonds), $S = 1.83$ (squares), $S = 2.75$ (triangles), and $S = 4.13$ (circles). As in Fig. 3, the value of h^* has been normalized for ease of comparison.

of h^* and its asymptotic, high-f value—in other words, the variation in efficiency becomes more pronounced for higher S. This observation holds true for all systems tested, although "saturation" is inevitably reached in all cases, where a further increase in S will no longer lead to a greater difference between the extremal h^* values. The increased "decay rate" of h^* with Γ for larger driving energy inputs, S, can perhaps be explained by the fact that for higher values of S, a change in Γ at constant S will result in a larger change in the driving amplitude, A, as compared to the same $\Delta\Gamma$ for the case of a smaller S value. Since, as discussed above and exemplified in Fig. 4, the collision rate and hence magnitude of base-bed energy transfer is directly dependent on A, it seems reasonable that higher S systems should see a more rapid relative decrease in h^* with increasing Γ (and therefore, since $S = \text{const.}$, decreasing A) than similar but more weakly excited systems.

For a system with a given, fixed depth, N_L, the breakdown of the monotonic increase of h^* with increasing A (i.e., *decreasing* Γ) at large A (small Γ) may perhaps be explained in the following manner: as the nondimensionalized driving acceleration, Γ, tends toward unity—the minimal value for which a mass on an oscillating plate may achieve "free flight" (i.e., detachment from the vibrating base) [46]—one would expect the normally fluidized bed to approach a solid-like state. More specifically, as Γ is lowered, an increasing proportion of the bed's constituent particles are likely to "condense" [47] into a solid body and begin to exhibit coordinated motion with the system's vibrating base, as opposed to the random, fluid-like motion observed at higher accelerations. Evidence for such a transition may be observed in Fig. 8; here we see experimental power spectra corresponding to time-dependent variation in z position of the vertical mass center of a system with fixed $N_L = 6$ driven at a constant $S = 1.83$. This specific value of S is achieved using three differing combinations of f, A, and hence, Γ.

The power spectra shown in Fig. 8 are acquired simply by taking the fast Fourier transform (FFT) of the experimental tracer particle's motion in the z direction over the course of a data set. If data is acquired over a period of time adequate to allow the tracer to fully explore the system in question (as is the case here—see Sec. II B), any cyclic motion of the system's vertical center of mass will be represented in the FFT data [48]: if the particles within the system undergo some degree of periodic, collective motion in the vertical direction, the tracer will

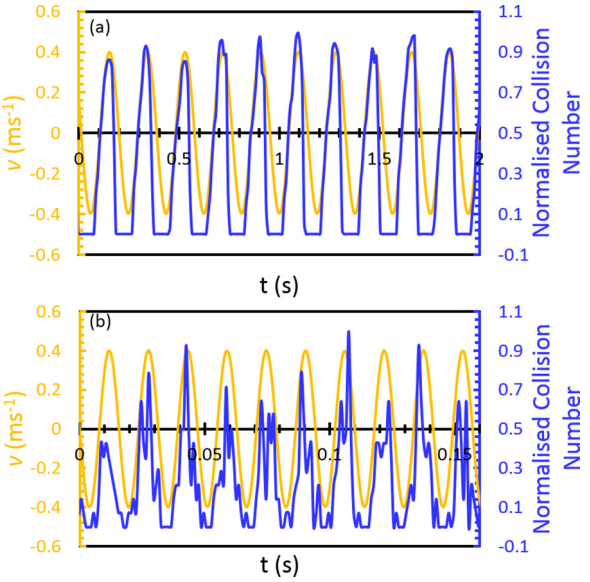

FIG. 7. (Color online) Number of particle collisions as a function of time for two simulated systems of identical resting depth $N_L = 3$ driven with equal dimensionless input energies, $S = 3.26$, achieved using frequency-amplitude combinations of (a) $A = 12.0$, $f = 5.31$ ($\Gamma = 1.36$) and (b) $A = 1.0$, $f = 63.7$ ($\Gamma = 16.3$). For each point in time, the collision number is shown alongside the instantaneous velocity of the vibrating base-plate, which forms the system's energy source. For ease of comparison, the collision number is normalized such that its maximal value is equal to unity.

become frequently "caught up" in the movement, creating a peak at the characteristic frequency of this motion in the power spectrum produced. As exemplified in the image, for values of A for which the simple increase of h^* with A is observed (see Fig. 2), the relevant power spectrum shows no distinct peaks, implying a randomized, fluid-like motion within the system. For higher A values, corresponding to lower Γ, however, it becomes possible to distinguish a definite peak at a frequency corresponding to that of the system's driving, indicative of the fact that the dynamics of at least some of the particles in the system have become coordinated with the base's oscillatory motion, as hypothesized. Moreover, as A is further increased (i.e., Γ is further decreased toward unity), the magnitude of the observed peak is found to increase, indicating an increased degree of coherent motion within the bed, i.e., that a greater number of particles has indeed entered solid body motion.

Further evidence of the varying degrees of coordinated motion for differing Γ values may be seen in Fig. 7, which compares, over ∼10 oscillation cycles, the number of plate-particle collisions to the current velocity with which the plate is moving for two systems identical in terms of their N_L and S values, but differing in the applied acceleration, Γ. For the low-Γ case, as expected from the above discussion, we see a strong correlation between base and particle motion, and evidence of a coherent, coordinated motion of the bed as a whole. In particular, one may observe considerable, regular time periods during which no particle-base collisions are found to occur, indicating that the entire bed has entered a period of free flight. In other words, the bed's dynamics are approaching those of a single, solid body bouncing on a plate. The dynamics

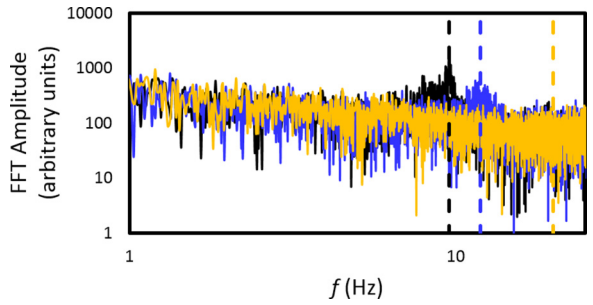

FIG. 8. (Color online) Experimentally acquired power spectra for the center of mass motion of a granular bed of depth $N_L = 6$ driven with input energy $S = 1.83$. This value of S is achieved using three differing combinations of driving frequency, f, and dimensionless amplitude, A/d: $f = 9.55$, $A/d = 1$ (black), $f = 11.9$, $A/d = 0.8$ (blue/dark gray), and $f = 19.9$, $A/d = 0.48$ (orange/light gray). Vertical dashed lines are used to demarcate the positions of the relevant driving frequencies.

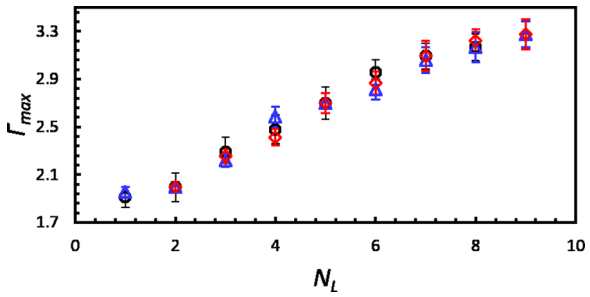

FIG. 9. (Color online) Simulated data showing the variation with bed depth, N_L, of $\Gamma_{\max}$, the value of the dimensionless acceleration at which, for a given N_L, energy transfer is maximal. Data is shown for input energies $S = 1.83$ (circles), $S = 4.13$ (triangles), and $S = 7.34$ (diamonds).

of the comparatively high-Γ system, however, are considerably more chaotic; although, for obvious reasons, the collision rate is typically reduced during the downward portion of the plate's motion and increased during the upward phase, the timing and number of collisions is, in general, much more randomized and less periodic.

The apparent change of state from a granular fluid to a more solid-like phase suggested by the behaviors discussed above may well (due to the more rapid dissipation of energy in an increasingly dense state [49,50]) explain the curtailment of the increasing trend between h^* and A. In other words, despite the fact that as A is increased (and hence Γ decreased), the mean *particle-base* collision rate, and thus kinetic energy provided to the system continues to grow, this increase is offset, and eventually dominated, by the rapid increase in the dissipation arising from the bed's higher packing density and hence *interparticle* collision frequency. Indeed, for the low-Γ case, we clearly see from Fig. 7 that the maxima in particle collision rate are consistently observed to coincide with the points in time at which the energy-providing plate reaches its peak positive velocity, i.e., the energy *input* to the system is clearly increased compared to higher-Γ systems. However, as discussed above, the increasingly synchronized nature of the particles' motion with decreasing Γ also leads to a greatly increased particle collision rate and, as a result, an increased dissipation, which, in the extremal case, will result in inelastic collapse [51,52] and a system of particles that simply behaves as a single, perfectly inelastic ball [53–55], pseudoinstantaneously dissipating all energy provided to it. The behavior of systems in and approaching this limit is discussed in detail in Ref. [56].

The above hypothesis can also explain the observed shift in the position of the maximum in h^* versus Γ for differing N_L values (see Fig. 9), since the increased dissipation caused by the addition of extra particles to a system is known to raise the onset threshold for fluidization in vibrated granular systems [57]. The simulated data in Fig. 9 also provide further support for the invariance of the position of this maximum with input energy as illustrated for the $N_L = 3$ case in Fig. 6, demonstrating the generality of this observation—for each of the N_L values tested, the "peak" value of the dimensionless acceleration, $\Gamma_{\max}$, at which the system's behavior switches from increasing with A to decreasing with A was found to remain constant to within the appropriate error margins over a range of S values. Indeed, this seeming invariance was observed for all tested S values for which the system's behavior was found to display the characteristic curve described throughout this manuscript. This observation strongly suggests Γ to be the relevant energy-input control parameter determining the point at which maximal energy transfer may be achieved in a given vibrated granular system. This is an important result with clear practical applicability, as a knowledge of the key parameters underlying energy transfer may, for instance, prove useful in assessing the optimal operating points of industrial equipment.

Simulations were also conducted for varying values of the container width, $L_{x,y}$, in order to assess the applicability of our findings to systems of different sizes. Simulations were produced, for various N_L values, using systems of width $L_{x,y}/d \in (4,48)$—i.e., systems ranging from $\frac{1}{4}$ to 3 times the width of the experimental domain. An example of the results obtained may be seen in Fig. 10. It is first worth noting that the general, qualitative form of the relationship between h^* and Γ remains consistent for all tested $L_{x,y}$ values. Moreover, the value of $\Gamma_{\max}$, the acceleration value producing maximal energy transfer, appears, for a given N_L, to be invariant with system size for containers of horizontal extent $L_{x,y}/d \gtrsim 8$.

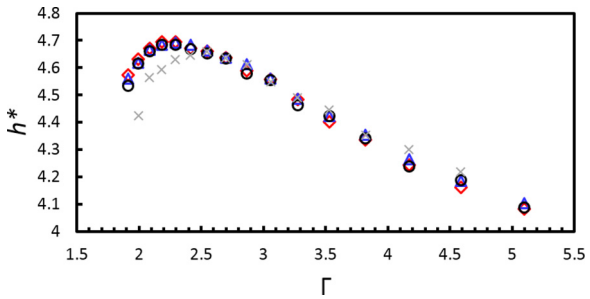

FIG. 10. (Color online) Simulated data showing relative center of mass position, h^*, as a function of dimensionless acceleration, Γ, for the case $N_L = 2$ and $S = 4.13$. Data is shown for systems of horizontal dimensions $L_{x,y}/d = 4$ (gray crosses), 16 (black circles), 24 (blue triangles), and 48 (red diamonds), corresponding to particle numbers, N, of 32, 512, 1152, and 4608, respectively.

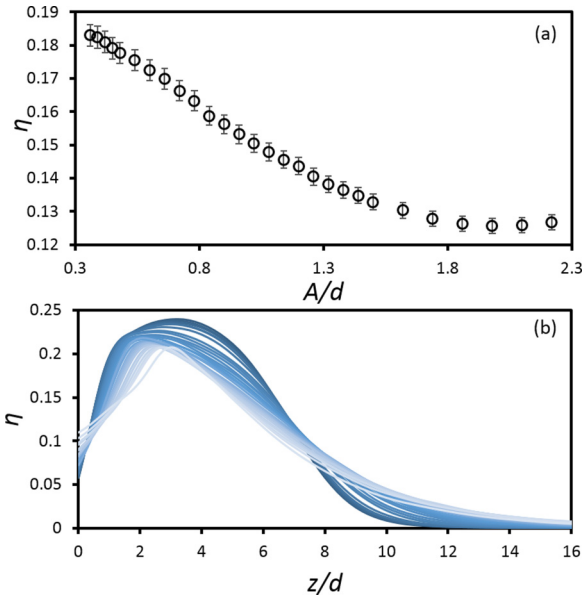

FIG. 11. (Color online) Variation in solids fraction, η, with driving parameters f and A for a fixed energy input $S = 3.26$ and bed depth $N_L = 3$, as obtained from simulations. Panel (a) shows the variation in the bed's *average* packing density as the amplitude, A, of driving is varied at fixed S. Panel (b), meanwhile, shows the one-dimensional vertical packing profiles corresponding to each data point in (a). In this image, lighter shades represent higher A or, equivalently, lower f.

The deviation observed in relatively narrow systems can likely be related to the greater acceleration necessary for the bed to become "detached" from the vibrating plate due to the considerably increased role of sidewall friction in more horizontally constrained beds [36,58]. Since holding the number of particle layers, N_L, constant while increasing the system's size will naturally require a larger total number of particles, N, our results clearly demonstrate that N_L, as opposed to N, acts as the 2nd relevant control parameter determining optimal energy transfer.

Accompanying the observed variation in the system's energy is, as one might expect, a modification of the bed's average packing fraction, η. An example of the variation in the average η for the $N_L = 3, S = 1.83$ case may be seen in Fig. 11(a). Figure 11(b), meanwhile, illustrates the fact that alongside the variation in *average* density, the *spatial distribution* of η also varies considerably with the differing combinations of f and A. Although outside the main interest of the current study, these variations in packing density may have significant implications, in particular for bi- and polydisperse systems. The separation and/or mixing of such systems is a matter of great industrial and environmental relevance [11,59,60], and the degree to which such segregation or homogenization is achieved depends strongly on η, making this an area worthy of further research.

IV. SUMMARY AND CONCLUSIONS

Using a combination of experimental and simulational techniques, we have investigated the behavior of a granular bed fluidized by contact with a vibrating plate, and the dependence of this behavior on the frequency, f, and amplitude, A, of the plate's oscillation.

We have shown that, for a given, fixed driving energy, $S = \frac{4\pi^2 f^2 A^2}{gd}$, the proportion of this energy actually transferred to the system being energized may be *significantly altered* through careful choice of the parameters f and A.

The general forms for the variation in the efficiency of energy transfer as a function of driving frequency, amplitude, and acceleration have been demonstrated and shown to be robust over a range of system parameters. An explanation of the mechanisms underpinning these general trends has also been proposed.

We have established the key control parameters, $\Gamma = \frac{4\pi^2 f^2 A}{g}$ and N_L, underlying the efficiency of energy transfer to a vibrofluidized granular system, and determined the points in Γ-N_L phase space for which maximal efficiency is achieved.

Additionally, we have demonstrated that the variation of f and A at fixed S can strongly influence the average packing density of a system, as well as the spatial distribution of particles.

The findings of this work carry numerous ramifications of potential significance to both industry and research. As described above, a system with a given, fixed input energy may possess a significant range of internal energies, densities, and even dynamic states dependent on the precise details of its driving. This observation raises serious questions as to the reliability and accuracy of any studies (past or future) detailing the variation of a system's behavior with driving energy if care is not taken to ensure generality across a range of f and A values.

On a more positive note, the knowledge that energy transfer from a vibrating plate into a granular system may be rendered considerably more efficient for certain combinations of A, f, and N_L is potentially relevant to a variety of practical applications. For example, in the industrial sector, where vibration is used to process granulates, it may be possible to design and utilize equipment in a manner that maximizes energy efficiency and, hence, minimizes cost. Alternatively, a knowledge of how the number of particles in a system affects its energy absorption characteristics may aid the creation of more efficient granular dampers, a technology with a broad range of applications in fields as diverse as power tool manufacture and aerospace engineering [12,61–64].

The fact that, in addition to its internal energy, the packing density of a system—and the spatial distribution thereof—may also be altered at fixed S has considerable implications for multicomponent systems. In such systems, the degree of segregation or mixing between particles of different sizes or material properties may potentially be altered without the necessity of providing greater energy to the system—a possibility worthy of future research.

ACKNOWLEDGMENTS

The authors thank Chris de Jong of the University of Twente for the application of his computing expertise. The authors also gratefully acknowledge financial support from the Hawkesworth Scholarship, without which this work would not be possible.

[1] P. A. Johnson and X. Jia, Nonlinear dynamics, granular media and dynamic earthquake triggering, Nature **437**, 871 (2005).

[2] R. M. Iverson, The physics of debris flows, Rev. Geophys. **35**, 245 (1997).

[3] C. H. Scholz, Earthquakes and friction laws, Nature **391**, 37 (1998).

[4] L. T. Fan, Y.-M. Chen, and F. S. Lai, Recent developments in solids mixing, Powder Technol. **61**, 255 (1990).

[5] S. J. Antony, W. Hoyle, and Y. Ding, *Granular Materials: Fundamentals and Applications* (Royal Society of Chemistry, London, 2004).

[6] H. M. Jaeger, S. R. Nagel, and R. P. Behringer, Granular solids, liquids, and gases, Rev. Mod. Phys. **68**, 1259 (1996).

[7] A. D. Rosato, D. L. Blackmore, N. Zhang, and Y. Lan, A perspective on vibration-induced size segregation of granular materials, Chem. Eng. Sci. **57**, 265 (2002).

[8] S.-S. Hsiau, C.-C. Liao, P.-Y. Sheng, and S.-C. Tai, Experimental study on the influence of bed height on convection cell formation, Exp. fluids **51**, 795 (2011).

[9] D. U. Ringer and A. S. Mujumdar, Analysis of aerodynamics and heat transfer in vibro-fluidized beds, Drying Technol. **2**, 449 (1983).

[10] S. Satija and I. L. Zucker, Hydrodynamics of vibro-fluidized beds, Drying Technol. **4**, 19 (1986).

[11] N. Mohabuth, P. Hall, and N. Miles, Investigating the use of vertical vibration to recover metal from electrical and electronic waste, Minerals Eng. **20**, 926 (2007).

[12] M. Heckel, A. Sack, J. E. Kollmer, and T. Pöschel, Granular dampers for the reduction of vibrations of an oscillatory saw, Physica A: Stat. Mech. Appl. **391**, 4442 (2012).

[13] M. Saeki, Impact damping with granular materials in a horizontally vibrating system, J. Sound Vibration **251**, 153 (2002).

[14] C. Zeilstra, M. A. Van Der Hoef, and J. A. M. Kuipers, Simulation of density segregation in vibrated beds, Phys. Rev. E **77**, 031309 (2008).

[15] Q. Shi, G. Sun, M. Hou, and K. Lu, Density-driven segregation in vertically vibrated binary granular mixtures, Phys. Rev. E **75**, 061302 (2007).

[16] S. Luding, E. Clément, A. Blumen, J. Rajchenbach, and J. Duran, Studies of columns of beads under external vibrations, Phys. Rev. E **49**, 1634 (1994).

[17] S. Luding, H. J. Herrmann, and A. Blumen, Simulations of two-dimensional arrays of beads under external vibrations: Scaling behavior, Phys. Rev. E **50**, 3100 (1994).

[18] C. R. K. Windows-Yule and D. J. Parker, Center of mass scaling in three-dimensional binary granular systems, Phys. Rev. E **89**, 062206 (2014).

[19] J. A. C. Gallas, H. J. Herrmann, and S. Sokołowski, Convection cells in vibrating granular media, Phys. Rev. Lett. **69**, 1371 (1992).

[20] K. Windows-Yule and D. Parker, Density-driven segregation in binary and ternary granular systems, KONA Powder and Particle Journal (to be published).

[21] C. R. K. Windows-Yule, N. Rivas, and D. J. Parker, Thermal convection and temperature inhomogeneity in a vibrofluidized granular bed: The influence of sidewall dissipation, Phys. Rev. Lett. **111**, 038001 (2013).

[22] D. J. Parker, R. N. Forster, P. Fowles, and P. S. Takhar, Positron emission particle tracking using the new Birmingham positron camera, Nucl. Instr. Methods Phys. Res. Sec. A: Acceler. Spectrom. Detect. Assoc. Equip. **477**, 540 (2002).

[23] R. D. Wildman, J. M. Huntley, J.-P. Hansen, D. J. Parker, and D. A. Allen, Single-particle motion in three-dimensional vibrofluidized granular beds, Phys. Rev. E **62**, 3826 (2000).

[24] R. D. Wildman, J. M. Huntley, and D. J. Parker, Granular temperature profiles in three-dimensional vibrofluidized granular beds, Phys. Rev. E **63**, 061311 (2001).

[25] C. R. K. Windows-Yule and D. J. Parker, Boltzmann statistics in a three-dimensional vibrofluidized granular bed: Idealizing the experimental system, Phys. Rev. E **87**, 022211 (2013).

[26] R. D. Wildman, J. M. Huntley, and D. J. Parker, Convection in highly fluidized three-dimensional granular beds, Phys. Rev. Lett. **86**, 3304 (2001).

[27] C. R. K. Windows-Yule, T. Weinhart, D. J. Parker, and A. R. Thornton, Effects of packing density on the segregative behaviors of granular systems, Phys. Rev. Lett. **112**, 098001 (2014).

[28] Mercurydpm.org

[29] A. Thornton, T. Weinhart, S. Luding, and O. Bokhove, Modeling of particle size segregation: Calibration using the discrete particle method, Int. J. Modern Phys. C **23**, 1240014 (2012).

[30] A. R. Thornton, T. Weinhart, V. Ogarko, and S. Luding, Multi-scale methods for multi-component granular materials, Comput. Methods Materials Sci. **13**, 1 (2013).

[31] A. R. Thornton, D. Krijgsman, A. te Voortwis, V. Ogarko, S. Luding, R. Fransen, S. Gonzalez, O. Bokhove, O. Imole, and T. Weinhart. *DEM 6: Proceedings of the 6th International Conference on Discrete Element Methods and Related Techniques* (Colorado School of Mines, 2013), p. 393.

[32] M. Y. Louge, http://grainflowresearch.mae.cornell.edu/impact/data/Impact

[33] S. Warr, J. M. Huntley, and G. T. H. Jacques, Fluidization of a two-dimensional granular system: Experimental study and scaling behavior, Phys. Rev. E **52**, 5583 (1995).

[34] S. Aumaître and S. Fauve, Collision frequencies and energy flux in a dilute granular gas, Phys. Rev. E **73**, 010302 (2006).

[35] E. Falcon, S. Aumaître, P. Evesque, F. Palencia, C. Lecoutre-Chabot, S. Fauve, D. Beysens, and Y. Garrabos, Collision statistics in a dilute granular gas fluidized by vibrations in low gravity, Europhys. Lett. **74**, 830 (2006).

[36] P. Eshuis, K. Van Der Weele, D. Van Der Meer, R. Bos, and D. Lohse, Phase diagram of vertically shaken granular matter, Physics Fluids **19**, 123301 (2007).

[37] S. McNamara and E. Falcon, Simulations of vibrated granular medium with impact-velocity-dependent restitution coefficient, Phys. Rev. E **71**, 031302 (2005).

[38] S. Aumaître, A. Alastuey, and S. Fauve, A quasi-elastic regime for vibrated granular gases, Eur. Phys. J. B: Condensed Matter Complex Systems **54**, 263 (2006).

[39] A. Sack, M. Heckel, J. E. Kollmer, F. Zimber, and T. Pöschel, Energy dissipation in driven granular matter in the absence of gravity, Phys. Rev. Lett. **111**, 018001 (2013).

[40] S. Warr, W. Cooke, R. C. Ball, and J. M. Huntley, Probability distribution functions for a single-particle vibrating in one dimension: Experimental study and theoretical analysis, Physica A: Stat. Mech. Appl. **231**, 551 (1996).

[41] S. Aumaître, J. Farago, S. Fauve, and S. McNamara, Energy and power fluctuations in vibrated granular gases,

Eur. Phys. J. B: Condensed Matter Complex Systems **42**, 255 (2004).

[42] V. Kumaran, Temperature of a granular material fluidized by external vibrations, Phys. Rev. E **57**, 5660 (1998).

[43] P. Sunthar and V. Kumaran, Characterization of the stationary states of a dilute vibrofluidized granular bed, Phys. Rev. E **64**, 041303 (2001).

[44] R. D. Wildman and J. M. Huntley, Scaling exponents for energy transport and dissipation in binary vibro-fluidized granular beds, Physics Fluids **15**, 3090 (2003).

[45] V. Zivkovic, M. J. Biggs, and D. H. Glass, Scaling of granular temperature in a vibrated granular bed, Phys. Rev. E **83**, 031308 (2011).

[46] D. Bachmann, *Verfahrenstechnik zvdi beiheft* (World Scientific, 1940).

[47] C. R. Wassgren, C. E. Brennen, and M. L. Hunt, Vertical vibration of a deep bed of granular material in a container, J. Appl. Mech. **63**, 712 (1996).

[48] C. R. K. Windows-Yule, N. Rivas, D. J. Parker, and A. R. Thornton, Low-frequency oscillations and convective phenomena in a density-inverted vibrofluidized granular system, Phys. Rev. E **90**, 062205 (2014).

[49] A. Kudrolli, M. Wolpert, and J. P. Gollub, Cluster formation due to collisions in granular material, Phys. Rev. Lett. **78**, 1383 (1997).

[50] J. S. Olafsen and J. S. Urbach, Clustering, order, and collapse in a driven granular monolayer, Phys. Rev. Lett. **81**, 4369 (1998).

[51] S. McNamara and W. R. Young, Inelastic collapse and clumping in a one-dimensional granular medium, Phys. Fluids A: Fluid Dynam. **4**, 496 (1992).

[52] L. P. Kadanoff, Built upon sand: Theoretical ideas inspired by granular flows, Rev. Modern Phys. **71**, 435 (1999).

[53] F. Melo, P. B. Umbanhowar, and H.y L. Swinney, Hexagons, kinks, and disorder in oscillated granular layers, Phys. Rev. Lett. **75**, 3838 (1995).

[54] E. Van Doorn and R. P. Behringer, Dilation of a vibrated granular layer, Europhys. Lett. **40**, 387 (1997).

[55] M. Sánchez, G. Rosenthal, and L. A. Pugnaloni, Universal response of optimal granular damping devices, J. Sound Vibrat. **331**, 4389 (2012).

[56] C. R. K. Windows-Yule, A. D. Rosato, A. R. Thornton, and D. J. Parker, Resonance effects on the dynamics of dense granular beds: achieving optimal energy transfer in vibrated granular systems, New J. Phys. **17**, 023015 (2015).

[57] B. Thomas, M. O. Mason, Y. A. Liu, and A. M. Squires, Identifying states in shallow vibrated beds, Powder Technol. **57**, 267 (1989).

[58] J. Duran, *Sands, Powders, and Grains*, Vol. 12 (Springer, New York, 2000).

[59] F. J. Muzzio, T. Shinbrot, and B. J. Glasser, Powder technology in the pharmaceutical industry: The need to catch up fast, Powder Technol. **124**, 1 (2002).

[60] G. Metcalfe and M. Shattuck, Pattern formation during mixing and segregation of flowing granular materials, Physica A: Stat. Mech. Appl. **233**, 709 (1996).

[61] D. I. Ryzhkov, Vibration damper for metal cutting, Eng. Dig. (Toronto) **14**, 246 (1953).

[62] J. C. Norcross, Dead-blow hammer head, U.S. Patent 3, 343, 576 (1967).

[63] H. V. Panossian, Structural damping enhancement via non-obstructive particle damping technique, J. Vibrat. Acoust. **114**, 101 (1992).

[64] S. S. Simonian, Particle damping applications, Proceedings of the 45th AIAA/ASME/ASCE/AHS/ASC Structures, Structural Dynamics & Materials Conference, 2004, p. 1906.